A Fluid Experiment of Large-Scale Topography Effect on Baroclinic Wave Flows①

Guoqing Li (李国庆)
Institute of Atmospheric Physics, Academia Sinica, Beijing, China
Robin Kung
Geophysical Fluid Dynamics Institute, Florida State University, Tallahassee, Florida, U. S. A.
and *Richard L. Pfeffer*
Geophysical Fluid Dynamics Institute and Department of Meteorology, Florida State University, Tallahassee, Florida, U. S. A.
Received February 2, 1991; revised July 30, 1991

ABSTRACT

The effects of topography on baroclinic wave flows are studied experimentally in a thermally driven rotating annulus of fluid.

Fourier analysis and complex principal component (CPC) analysis of the experimental data show that, due to topographic forcing, the flow is bimodal rather than a single mode. Under suitable imposed experimental parameters, near thermal Rossby number $R_{OT} = 0.1$ and Taylor number $T_a = 2.2 \times 10^7$, the large-scale topography produces low-frequency oscillation in the flow and rather long-lived flow pattern resembling blocking in the atmospheric circulation. The 'blocking' phenomenon is caused by the resonance of travelling waves and the quasi-stationary waves forced by topography.

The large-scale topography transforms wavenumber-homogeneous flows into wavenumber-dispersed flows, and the dispersed flows possess lower wavenumbers.

I. INTRODUCTION

Because of the zonal asymmetric distribution of the earth's large-scale topography, such as the Himalayas and the Rocky Mountains, long-term mean waves in the mid-latitudes exist (Charney and Eliassen, 1949; Bolin, 1950). Some scientists believe that under favorable conditions, the interaction of topographically forced waves with slowly moving free waves may lead to development of blocking highs in the troposphere (e.g., Egger, 1978; Tung and Lindzen 1979). Charney and Devore (1979) and Hart (1979) suggested that, for given forcing parameters, multiple stable steady states of the zonal-mean wind and planetary wave amplitude were possible due to the topographically induced instability in a simple barotropic model. Other works illustrated similar possibilities in baroclinic models (e.g., Charney and Strauss, 1980; Pedlosky, 1981; Reinhold and Pierrehumbert, 1982). In these models, one stable steady state corresponds to a relatively strong zonal flow, while another corresponds to a state with a weak zonal flow and a wave pattern resembling blocking. These results indicate that the quasi-geostrophic model, in which the spherical Earth is replaced by the β plane,

①This research was supported by the U.S. National Science Foundation Grants ATM-8709410 and ATM-8714674.

can successfully model many of the essential features of the general atmospheric circulation. This suggests that the fundamental properties of the general atmospheric circulation are not dependent on the spherical geometry or other parameters unique to the Earth, but may be common to all rotating differentially heated fluids. If so, the discussed phenomena could exist in rotating systems in the laboratory. In fact, many laboratory experiments have been done in recent years which simulate important processes in the general atmospheric circulation (e.g., Fultz et al., 1959; Hide and Mason, 1975; Yeh and Chang, 1974; Research Group on Experimental Simulation, Institute of Atmospheric Physics, Academia Sinica, PRC, 1978; Pfeffer et al., 1974, 1980; Bernardent et al., 1991). Recently, Pfeffer has managed a series of laboratory experiments which intend to simulate the influence of large–scale topography on atmospheric circulation(1986, 1989, 1990). The present work is a continuation of this research.

In Section 2 we shall describe the experimental apparatus and methodology of the experiment. In Section 3, we shall discuss the bimodality and the low–frequency oscillation in the baroclinic flow forced by large–scale topography and compare it with the Earth's atmospheric circulation. In Section 4, we shall delineate the resonant behavior in the interaction of the slowly travelling waves and the topographically forced waves. In Section 5, we shall discuss the wavenumber dispersion in the flow aroused due to large–scale topography forcing. The conclusions will be given in Section 6.

II. EXPERIMENTAL APPARATUS AND METHOD

A sketch of the experimental annulus is shown in Fig.1. The basin B is filled with 5 centistoke silicon fluid with a depth of 10 cm measured from the middle of the mountain. A constant temperature difference, $\triangle T = T_2 - T_1$, between the outer and inner brass walls of the basin is maintained by circulating warm water in bath A and cold water in bath C. The outer radius of the inner brass cylinder is $a = 7.5$ cm and the inner radius of the outer brass cylinder is $b = 15$ cm. In order to visualize the horizontal flow, we used a kind of streak photography wherein white polyethylene particles were used as tracers. These particles were illuminated by a laser beam. From the lengths of the trajectories traversed by the tracers and the exposure time, the fluid velocity could be obtained. The photographs were digitized to put the data in numerical form and azimuthal (u) and radial (v) velocity components were calculated from the data. Using u and v components of velocity, we were able to evaluate many characteristic features of the flow fields by doing both Fourier and complex principal component (CPC) analyses.

We used a two–sinusoidal wave topography, which can be described by the formula

$$h = H\cos 2\lambda \ , \tag{1}$$

where $h(\lambda)$ is the topographic height, $H = 1.75$ cm, and λ, $0 \leqslant \lambda \leqslant 2\pi$, is the azimuthal angle measured counterclockwise, from one of the ridges.

In the earlier experiments, the bottom surface of the annulus was latitudinally flat and the β–effect was produced only by slope of the free surface due to rotation. The β–effect produced in this way is very small when the rotation rate is small and significant at high rotation rates. In later experiments, we used a topography with a 20° latitudinally sloped annulus bottom surface to simulate the β–effect. The shape of this topography can be described by the formula

$$h = H\cos 2\lambda - (R - a)\tan\theta, \tag{2}$$

where R, $b > R > a$, is the radial distance from the axis of rotation to the point considered

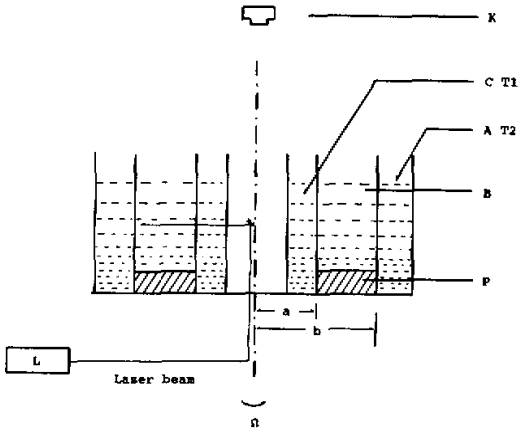

Fig.1. Schematic diagram of the apparatus. A–warm water with temperature T2, C–cold water with temperature T1, B–experimental area. K–camera. L–laser. P–topography, a = 7.5 cm, b = 15.0 cm.

and θ is the slope angle of the bottom surface. The β parameter can be evaluated by the formula

$$\beta = \frac{f}{D_0}\left(\left|\frac{\partial h_T}{\partial R}\right| + \left|\frac{\partial h_B}{\partial R}\right|\right), \tag{3}$$

where $\partial h_T / \partial R$ is determined by the centrifugal force due to the annulus rotation and $\partial h_B / \partial R$ is determined by the radial slope of the bottom surface, D_0 is the mean depth of the fluid, $f = 2\Omega$ is the Coriolis parameter, and Ω is the angular velocity of the rotation. In some of the experiments, we use the topography with a 20° latitudinal slope, and the β can be calculated by the formula.

$$\beta = \frac{2\Omega^3 R}{g D_0} + \frac{2\Omega}{D_0}\tan 20^o \ . \tag{4}$$

The values of terms $\beta_1 = 2\Omega^3 R / g D_0$ and $\beta_2 = 2\Omega \tan 20^o / D_0$ calculated for different rotation rates are shown in Table 2. It shows that the values of β are determined mainly by the slope of the bottom surface rather than centrifugal force.

If we use the expression

$$\beta^* = \frac{\beta L^2}{v}, \tag{5}$$

where L is the horizontal characteristic length and v is the characteristic velocity of the motion, we can evaluate β^* in a dimensionless form. Choosing $\beta = 0.1 \mathrm{cm}^{-1}\mathrm{s}^{-1}$ for the experiment and $\beta' = 1.14 \times 10^{-11}\mathrm{m}^{-1}\mathrm{s}^{-1}$ for the atmosphere, we find that $\beta_a^* = 0.95 \times 10^2$ for the atmosphere and $\beta_e^* = 1.25 \times 10^3$ for the experiment. It shows that the value of β is larger even in the experiment.

To understand the gross features of the general circulation, the quasi–geostrophic model

can be used. The previous laboratory experiments show that, for certain combination of rotation and differential heating rates, the annulus flow follows the geostrophic relationship, the thermal wind relationship with the radial temperature gradient, and the hydrostatic relationship,

$$2\Omega U = \frac{K\nabla P}{\rho_0} , \tag{6}$$

$$\frac{\partial U}{\partial Z} = \frac{\alpha g}{2\Omega} K \times \nabla T , \tag{7}$$

$$\frac{\partial P}{\partial Z} = -\rho_0 g , \tag{8}$$

where K is the unit vector along z axis, U the geostrophic velocity of the fluid, ∇P the pressure gradient, ∇T the temperature gradient between the walls, α the coefficient of volume expansion of the fluid, and ρ_0 the mean density of the fluid. This ensures that the mathematical analysis of the experiments can proceed from the same equations which describe the atmosphere, except that cylindrical geometry replaces spherical geometry and temperature replaces potential temperature in the thermal equation because the annulus fluid is incompressible and adiabatic temperature change can be neglected.

In the experiments, the geostrophy of the flows depends on the imposed Rossby number,

$$R_{OT} = \frac{\alpha g D_0 (T_b - T_a)}{2\Omega^2 (b-a)^2} , \tag{9}$$

and the Taylor number,

$$T_a = \frac{4\Omega^2 (b-a)^4}{v^2} , \tag{10}$$

where $\alpha = 1.05 \times 10^{-3} c^{-1}$ is the coefficient of volume expansion of the fluid and $v = 5 \times 10^{-6} m^2 s^{-1}$ is kinematic viscosity of the fluid.

Therefore, we can model the gross features of the general atmospheric circulation using rotating fluid experiment.

Table 1. Dimensional Parameters Related to the Experiments

Atmosphere		*Experiments*	
$R' = 6.37 \times 10^6 m$	mean radius of the Earth	$R = 1.12 \times 10^{-1} m$	mean distance from the axis of annulus rotation
$\Omega' = 7.29 \times 10^{-5}$ rad s^{-1}	angular velocity of Earth's rotation	$\Omega = 0.31 \sim 3.14$ rad s^{-1}	angular velocity of the annulus rotation
$n' = 2$	number of stationary waves	$n = 2$	number of stationary waves
$L' = 2\pi R' / n'$ $= 2.0 \times 10^7 m$	characteristic length	$L = 2\pi R / n$ $= 3.53 \times 10^{-1} m$	characteristic length
$g = 9.81 ms^{-2}$	gravity acceleration	$g = 9.81 ms^{-2}$	gravity acceleration
$v' = 1.5 \times 10^4 m^2 s^{-1}$	eddy viscosity of the atmosphere	$v = 5 \times 10^{-6} m^2 s^{-1}$	kinematic viscosity of the fluid
$H' = 1.2 \times 10^4 m$	mean height of the atmosphere	$D_0 = 0.1$ m	mean depth of the fluid

Table 2. The Values of β and Its Components for Different Rotation Rates

$\Omega[s^{-1}]$	0.490	0.628	0.785	1.050	1.570	2.100	3.140
$\beta_1 \times 10^{-2}[cm^{-1}s^{-1}]$	0.027	0.114	0.222	0.531	1.780	4.520	14.20
$\beta_2 \times 10^{-2}[cm^{-1}s^{-1}]$	3.570	4.570	5.710	7.640	11.40	15.30	22.90
$\beta \times 10^{-2}[cm^{-1}s^{-1}]$	3.600	4.680	5.930	8.170	13.20	19.60	37.10

III. BIMODALITY AND LOW-FREQUENCY OSCILLATION IN TOPOGRAPHICALLY FORCED FLOW

Whether the large-scale atmospheric circulation undergoes temporal variations of more than one regime is an important question. If more than one regime exists in the atmospheric circulation, then the mean state of the atmosphere would not be represented by its long-term average, but by the set of average states obtained by each individual regime. This question has received more attention in recent years. We try to study this question using the results of the fluid experiments.

The sequences of the streamfunction patterns corresponding to an experiment with topographic forcing are presented in Fig.2. In the figure, the arrows and their opposites indicate the mountain peaks. Comparing the flow patterns with each other, we classify all the patterns into two dominant modes. Mode 1, patterns 1–7 and 17–19, is characterized by strong zonal flows with well developed troughs located in the topographic valleys. Mode 2, patterns 10–16, is characterized by weaker zonal flows and strong ridges or 'blocking' anticyclonic vortices located at the same areas. The mode of patterns 8 and 9 is unstable and transitional between the two above stated dominant modes. In Fig.3, we present the time-averaged pattern of the streamfunction for this experiment. In accordance with the distribution of the troughs and ridges in the flow pattern, it can be seen that neither of the dominant modes is alike to the time-averaged-pattern. Moreover, the evolution of the anticyclone-vortices at the areas between the mountains resembles the blocking process. Fig.2 shows that the blocking vortices form steadily at pattern 12 and strengthen as time goes on, reaching their mature stage at pattern 14. At pattern 15, the vortices become weaker and they disappear after pattern 17. These blocking vortices persist for about 33.4 annulus rotations. Later, we shall prove that this time-interval corresponds approximately to 7 days in the system of Earth's atmospheric circulation.

The experimental results show that topographic forcing plays a dominant role in the occurrence of these blocking-vortices because it is the only way we can explain why they form and maintain at fixed geographical localities. In the experiments with the same imposed parameters but without topographic forcing, we never observe this kind of flow vacillation and the blocking.

Let us now compare the oscillation frequency of the experimental flow and that of the atmospheric circulation using scale analysis and similarity principle. Taking the values of characteristic length and velocity from Table 1 for the considered experiment shown in Fig.2, we have $L=35.3$ cm and $u=0.1$ cm s^{-1}. The characteristic time for the experimental flow would be $t^* = L/u = 3.53 \times 10^2$ s. As the flow vacillates with a period of 127 rotations and the rotation period of the annulus is 3 seconds, so that the flow vacillation period would be $t=381$ s. The dimensionless value of the flow vacillation period would be $\hat{t} = t/t^* = 1.08$. For the Earth's atmosphere, if we take the characteristic length to be $L' = 2.0 \times 10^7$ m and the characteristic wind speed in the troposphere $\bar{u} = 10$ ms^{-1}, then the characteristic time

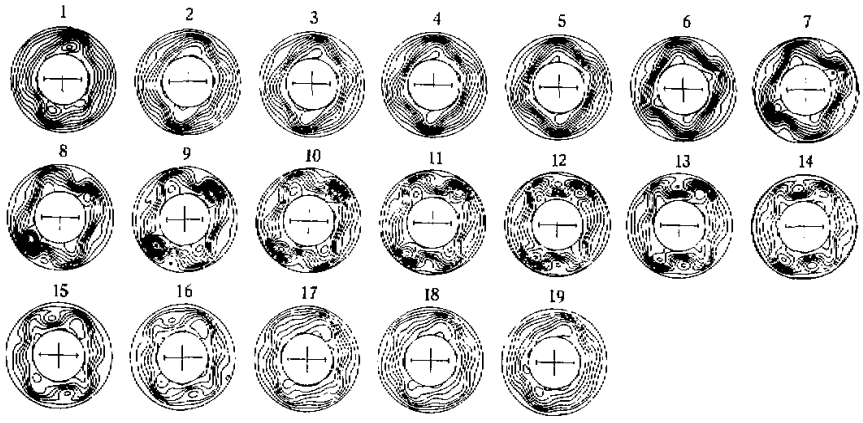

Fig.2. Sequences of streamfunction patterns corresponding to experiments with topographic forcing. The photo number is indicated next to each picture. Shading designates negative values. Contour intervals, 0.05 cm^2s^{-1}. The experimental parameters: $\Omega = 2.09\ s^{-1}$, $\triangle T = 2.0℃$. The mountain ridges are located at $\lambda = 0°$(arrow) and $\lambda = 180°$.

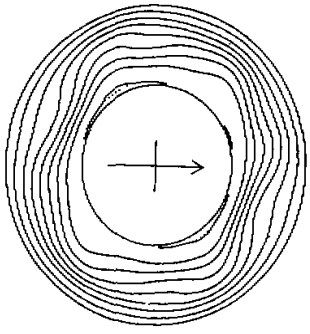

Fig.3. Same as Fig.2, but for time averaged pattern of streamfunction.

would be $t^{*'} = L'/u' = 2 \times 10^6$ s. As we have discussed, the experimental fluid system and the Earth's atmosphere resemble each other, therefore, vacillation period of the experimental flow would correspond to a value of time $t' = t^{*'} \times \hat{t} = 25$ days, i.e., the vacillation in the experimental flow corresponds to the low-frequency oscillation in the Earth's atmosphere. This may suggest that part of the reason for the low-frequency oscillation in the general atmospheric circulation lies in the forcing of large-scale topography.

Similarly, as mentioned before, the blocking vortices in the discussed experiment persist for 33.4 annulus rotations which corresponds to 7 days in the Earth system.

IV. RESONANT INTERACTION OF TRAVELLING WAVES WITH TOPOGRAPHY-FORCED WAVES

Now, we use some results of complex principal (CPC) analysis of the experimental data, the methodology of which was stated in detail by Pfeffer (1990), to reveal the interaction behavior of topographically forced quasi-stationary waves with slow-moving waves.

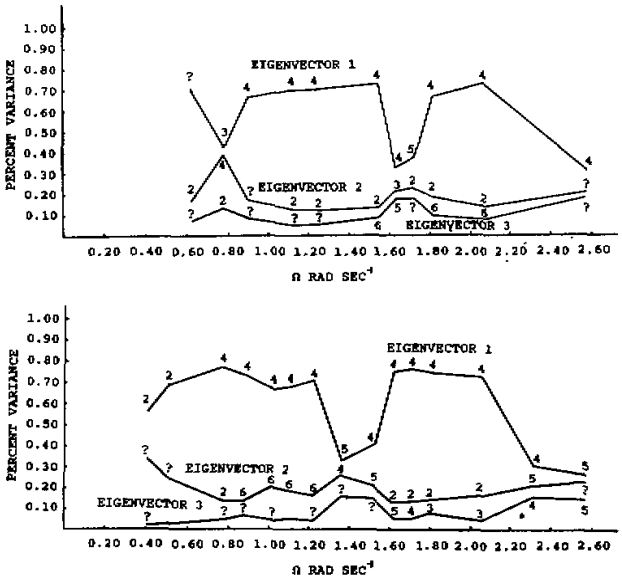

Fig.4. Percent variances of streamfunctions of the first three principal components of the flows in the experiments with topographic forcing. The ordinate represents fractional values of the variances. The abscissa represents the rotation rates in rad s^{-1}. The numbers indicate wavenumbers of the flows. $\triangle T \approx 2.0℃$. ? denotes chaotic flow.

a. For the flows at the level of 8.4 cm. b. For the flows at the level of 2.3 cm.

In Table 3, we present the percent variance of ψ', deviation of the time-averaged streamfunction, for the first three eigenvalues for the experiments with topographic forcing at different rotation rates. It shows that the variance values of ψ' for eigenvalue 1 decrease abruptly at some rotation rates. For instance, for eigenvalue 1, the variance is larger than 0.68 when $\Omega \leqslant 1.26\ s^{-1}$. It decreases to 0.377 at $\Omega = 1.40\ s^{-1}$ and 0.477 at $\Omega = 1.58\ s^{-1}$, it increases again, and exceeds 0.80 when $1.66\ s^{-1} \leqslant \Omega \leqslant 2.10\ s^{-1}$. Finally, it drops down to a value less than 0.3 at $\Omega = 2.36\ s^{-1}$. We need to know the reason for the abrupt decrease of the variance values of ψ' at some rotation rates.

In Fig.4. we present variances of streamfunctions for the flows at heights of 8.4 cm and 2.3 cm for the same series of experiments shown in Table 3. It is evident that all of the high values of the percent streamfunction variances of the first principal component correspond to a coincidence of two even wavenumbers of the first and the second principal components. For the low values of the percent variances of the streamfunctions, however, one of the first two principal components corresponds to an odd wavenumber and another to an even wavenumber. Certainly, two waves can match each other better when both of them have even wavenumbers, and the waves are stable and, therefore, the first principal component possesses a larger value of the percent variance of streamfunction. On the contrary, if one of these two principal components corresponds to an even wavenumber and another to an odd wavenumber the waves do not match each other, and they are unstable and, therefore, the first principal component possesses less value of the percent variance of streamfunction. Perhaps this is the reason for the abrupt decrease in the percent variance of ψ' at some rotation

rates as shown in Table 3. Besides, Fig.4 shows that the most favorable modes which match each other are the quasi–stationary waves of wavenumber 2 and travelling waves of wavenumber 4.

Let us now examine the time variance of streamfunction of the first and second principal components in the experiment with topographic forcing at parameters $\triangle T = 2.0°$ and $\Omega = 2.09 s^{-1}$. Fig.5a and Fig.5b show the time variance of streamfunctions at the middle circle of the annulus ($R = 11.2$ cm). The abscissa represents azimuthal angles of the annulus, in the counterclockwise direction, from one of the ridges of the topography. The ordinate represents time in unit of annulus rotations. The shaded areas represent streamfunctions with negative values. The dotted lines point to the time when the extreme values of streamfunction of the first principal component appear in Fig.5a, that is, the time when the 'blocking' vortices reach their mature stage. As illustrated in Figs.5a and 5b, the first principal component is a flow with four travelling waves and the second principal component is a quasi–stationary flow with two waves. The value of the streamfunction of the first principal component flow periodically vacillates while the travelling waves move forward. At the same time and with the same period of time , the quasi–stationary waves of the second principal component vibrate forward and back relatively to their mean positions, $\lambda_1 = 3\pi / 4$ and $7\pi / 4$.

In Fig.5c and Fig.5d, we present the phase speed and phase angle of the quasi–stationary waves of the second principal component. Prior to the formation of the extreme values of the streamfunction for the first principal component, large negative values of phase speed for the second principal component of the flow appear, so that the stationary waves shift back to their most 'west' positions, $\lambda \approx -\pi / 4$. Then, as the streamfunction of the first principal component decreases, the phase angles of the stationary waves gradually increase (see Fig.5a and Fig.5d). Apparently, this indicates that there is a resonance between the travelling waves and the quasi–stationary waves formed due to topographic forcing. The 'blocking' of the flow occurs due to the resonant interference between the travelling waves of the first principal component and the quasi–stationary waves of the second principal component of the flow.

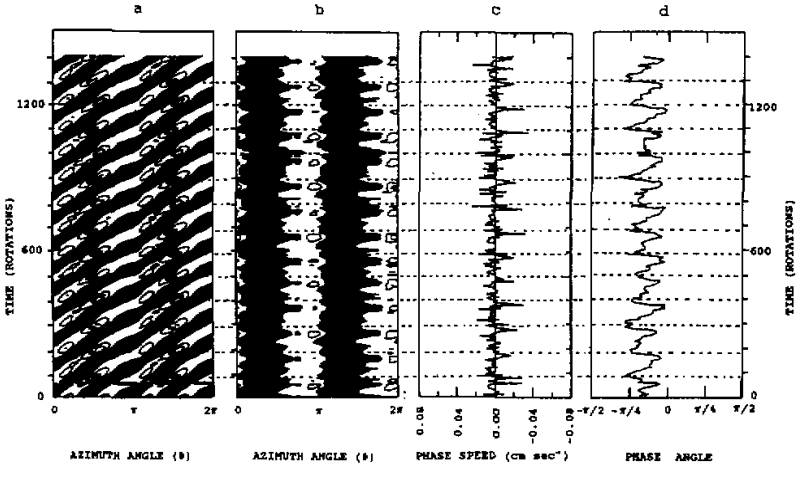

Fig.5. Time variance of streamfunctions along the middle circle (R = 11.2 cm) for the first (a) and second (b) principal components of the flow in the experiment with topographic forcing at $\Omega = 2.09$ s^{-1} and $\triangle T = 2.0℃$. Contour interval is 0.1 $cm^2 s^{-1}$. Negative values shaded. Time variance of phase speed (c) and phase angle (d) of the quasi–stationary waves of the second principal of the flow.

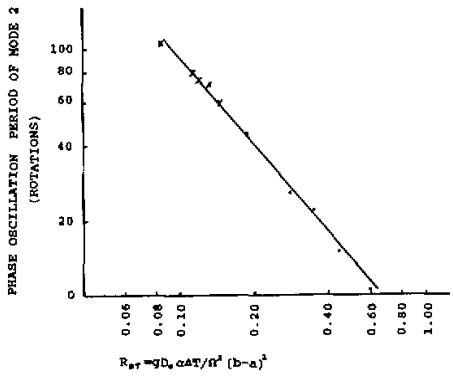

Fig.6. Oscillation period of the quasi-stationary waves versus the imposed thermal Rossby numbers. Mark x indicates the experiments with blocking.

Fig.6 shows the relationship of the vacillation period of stationary waves versus the imposed thermal Rossby numbers in the experiments with topographic forcing. According to this figure, the oscillation period of the stationary waves is inversely proportional to the imposed thermal Rossby number in the experiment. The blocking occurs only in a narrow area where R_{OT} is approximately equal to 10^{-1}. The mark x in Fig.6 indicates the experiments with blocking.

Table 3. Percent Variance of Streamfunction Deviation ψ' of the First Three Principal Components of the Flows at Level of 2.3 cm in the Experiments with Topographic Forcing. $\triangle T = 2.0$℃

$\Omega(s^{-1})$	Eigen 1	Eigen 2	Eigen 3
0.91	.750	.139	
1.05	.684	.206	
1.14	.712	.184	
1.26	.759	.145	
1.40	.377	.325	.114
1.58	.447	.244	.101
1.66	.836	.091	
1.75	.851	.084	
1.84	.841	.080	
2.10	.837	.073	
2.36	.298	.250	.157
2.62	.329	.208	.150
3.14	.304	.186	.173

V. WAVENUMBER DISPERSION

One of the phenomena we have found in these experiments is wavenumber dispersion of the travelling waves due to topographic forcing. In Fig.7, we present the curves showing the fractional values of the streamfunction variances and wavenumbers of the first two principal components of the flows at a height of 5.0 cm in a series of experiments without topographic

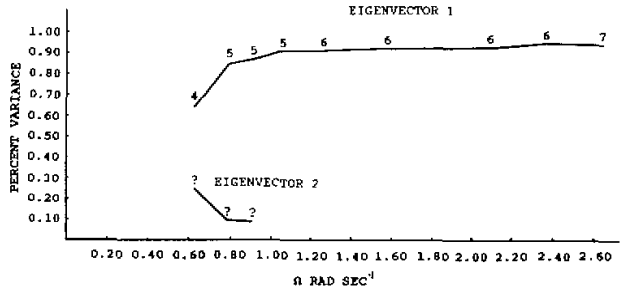

Fig.7. Same as Fig.4, but for the experiments without topographic forcing.

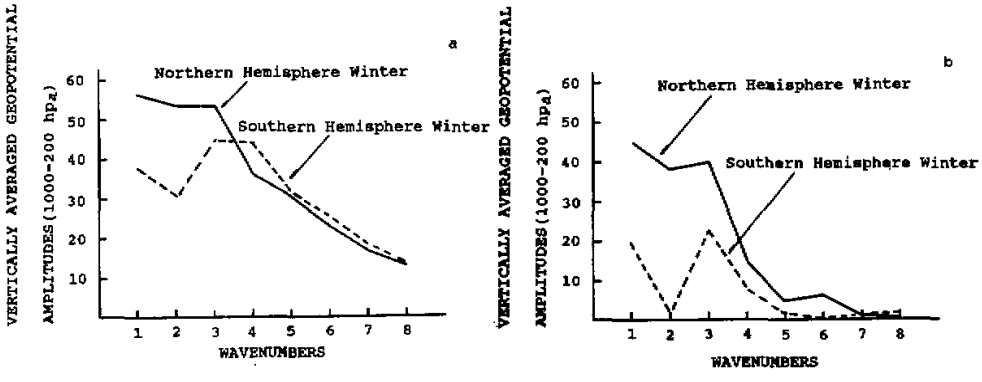

Fig.8. Winter time-mean planetary wave activity as revealed by vertically averaged (1000–200 hPa) geopotential amplitudes of wave components versus wavenumbers of longitudinal sinusoidal modes for the total wave amplitudes (a) and for the stationary wave components (b) in both Northern Hemisphere and Southern Hemisphere.

forcing. It shows that the values of the variances for the first principal components are pretty high for all experiments, except the one with $\Omega = 0.63\ s^{-1}$. All values of the variances for the first principal components are higher than 0.9 when $\Omega > 1.0\ s^{-1}$. This means that in the experiments without topography, the flows are comparatively wavenumber–homogeneous. Comparing Fig.4 and Fig.7 , we can see that in experiments without topographic forcing, most of the first principal components are flows of wavenumber 6. Due to topographic forcing, the values of streamfunction variances of the first principal components decrease and the second and the third principal components appear with rather high values of streamfunction variances. Also, the wavenumbers of the first principal components in the flows decrease due to the topographic forcing. Besides, Fig.4 shows that in the same experiment, the flow patterns at different levels are different.

The phenomenon of wavenumber–dispersion of the baroclinic waves due to topographic forcing in the experiments can be verified in the atmospheric circulation of the Earth. It is well

known that the Northern Hemisphere of the Earth differs greatly from the Southern Hemisphere in the amount and distribution of topography. The topographic effects on the atmospheric circulation should be more distinct in the Northern Hemisphere than those in the Southern Hemisphere. In Fig.8, we draw a few carves which show the winter time–mean planetary wave activity, as revealed by vertically averaged (1000–200 hPa) geopotential amplitudes of wave components versus wavenumbers of longitudinal sinusoidal modes. Fig.8 was drawn using ECMWF daily data from Dec. 1, 1979 to Dec. 31, 1985 analyzed by Buzzi and Tosi. The wave amplitudes were computed as the square root of the sum of squared sine and cosine components in longitude, for each latitudinal sinusoidal mode. Fig.8a provides information on total mean wave activity. It shows that the amplitude values in lower frequency area of wavenumbers 1, 2 and 3 are much higher in the Northern Hemisphere than those in the Southern Hemisphere. In the area of higher frequency of wavenumber larger than 4, the total wave amplitudes are a bit higher in the Southern Hemisphere than those in the Northern Hemisphere. Fig.8b shows the winter time mean amplitudes of the stationary components. It shows that the vertically averaged geopotential amplitudes are higher in the Northern Hemisphere for almost all wavenumbers. Especially, they are much higher in the low–frequency area of wavenumbers 1, 2 and 3 in the Northern Hemisphere than those in the Southern Hemisphere. All these facts perhaps show the different influences of large–scale topography on the atmospheric ciculation in both of the two hemispheres.

VI. CONCLUSIONS

The fluid experiments, despite their many idealizations, can model the most important features of the general atmospheric circulation. The fundamental effects of large–scale topography on baroclinic wave flows are as follows:

1) While the flow without topographic forcing is unimodal, the flow with topographic forcing is bimodal. Mode 1 is characterized by a strong zonal flow, and mode 2 is characterized by a meridionally disturbed flow. The large–scale topography produces low–frequency oscillation in the flow and rather long–lived vortices that resemble blocking highs in the atmospheric circulation.

2) The complex principal component (CPC) analyses of the experimental data show that there is an interaction of topographically forced quasi–stationary waves with slowly moving free waves. The resonant interference of these waves lead to occurrence of 'blockling' vortices. The favorable modes which match each other in this interference are of stationary waves of wavenumber 2 and travelling waves of wavenumber 4. However, the 'blocking' occurs only in a narrow area of the parameter space near thermal Rossby number $R_{OT}=0.1$ and Taylor number $T_a=2.2\times10^7$.

3) A phenomenon found in the experiments is wavenumber–dispersion of the travelling waves due to topographic forcing. The flows in the experiments without topographic forcing are of wavenumber–homogeneous. The large–scale topography transforms wavenumber –homogeneous flows to wavenumber–dispersed flows, increasing low–frequency components and decreasing high–frequency components of the flows.

The authors are grateful to Mr. Rene Arbogast for graphics programming, Mr. Gerald Arnord for his assistance in doing the laboratory experiments, and Mr. Clayton Lewis for his professional supervision of the digitizing personnel and painstaking data scrutiny and correction of errors.

REFERENCES

Benzi, R., P. Malguzzi, A. Speranza and A. Sutera (1986), The statistical properties of general atmospheric circulation: Observational evidence and a minimal theory of bimodality, *Quart. J. Roy. Met. Soc.*, **112:** 661–674.

Bernardent, P., A. Butet, M. Deque, M. Ghil and R.L. Pfeffer (1991), Low–frequency oscillation in a rotating annulus with topography, to be published in *J. Atmos. Sci.*

Bolin, B. (1950), On the influence of the earth's orography on the general character of the westerlies, *Tellus*, **2:** 184–195.

Buzzi, A. (1988), Low–frequency variability of atmospheric circulation: a comparison of statistical properties in both hemispheres and extreme seasons, Il Nuovo Cimento, 11C, N. 5–6.

Charney, J. G. and A. Eliassen (1949), A numerical method for predicting the perturbations of the middle latitude westerlies, *Tellus*, **1:** 38–54.

Charney, J.G. and J.G. Devore (1979), Multiple flow equilibria in the atmosphere and blocking, *J. Atmos. Sci.*, **36:** 1025–1216.

Charney, J.G. and D.M. Straus (1980), Form–drag instability, multiple equilibria and propagating planetary waves in baroclinic, orographically forced, planetary wave systems, *J. Atmos. Sci.*, **37:** 1157–1176.

Egger, J. (1978), Dynamics of blocking highs, *J. Atmos. Sci.*, **35:** 1788–1801.

Fultz, D., R.R. Long, G.V. Owens, W. Bohan, R. Kaylor and J. Weil (1959), Studies of thermal convection in a rotating cylinder with some implications for large–scale atmospheric motions, *Meteor. Monog.*, **21:** Amer. Met. Soc., 1–104.

Hart, J. E. (1979), Barotropic quasi–geostrophic flow over anisotropic mountains, *J. Atmos. Sci.*, **36:** 1736–1746.

Hide, R. and P.J. Mason (1975), Sloping convection in a rotating fluid, *Adv. Physics*, **24:** 47–100.

Li, G.–Q., R. Kung and R.L. Pfeffer (1986), An experimental study of baroclinic flows with and without two–wave bottom topography, *J. Atmos. Sci.*, **43:** 2585–2599.

Pedlosky, J. (1981), Resonant topographic waves in barotropic and baroclinic flows. *J. Atmos. Sci.*, **38:** 2626–2641.

Pfeffer, R.L., G. Buzyna and W.W. Fowlis (1974), Synoptic features and energetics of wave–amplitude vacillation in a rotating, differentially heated fluid, *J. Atmos. Sci.*, **31:** 622–645.

Pfeffer, R.L., G. Buzina and R. Kung (1980), Time dependent modes of behavior in thermally driven rotating fluids, *J. Atmos. Sci.*, **37:** 2129–2149.

Pfeffer, R.L., R. Kung and G.Q. Li (1989), Topographically–forced waves in a thermally driven rotating annulus of fluid–experiment and linear theory, *J. Atmos. Sci.*, **46:** 2331–2343.

Pfeffer, R.L., J. Ahlquist, R. Kung, G–Q. Li and Y. Chang, (1990), A study of baroclinic wave behavior over bottom topography using complex principal component analysis of experimental data, *J. Atmos. Sci.*, **47:** 67–81.

Reinhold, B.B. and R.T. Pierrehumbert (1982), Dynamics of weather regimes: Quasi–stationary waves and blocking, *Mon. Wea. Rev.*, **110:** 1105–1145.

Research Group on Experimental Simulation, Institute of Atmospheric Physics, Academia Sinica, PRC (1978), The annulus simulation of summer large–scale convective systems over the Qinghai–Tibetan Plateau, *Scientia Sinica.*, **21:** 347–364.

Tung, K.K. and R.S. Lindzen (1979), A theory of stationary long waves. Part 1: A simple theory of blocking, *Mon. Wea. Rev.*, **107:** 714–734.

Yeh, T.–C., and C.C. Chang (1974), A preliminary simulation on the heating effect of the Tibetan Plateau on the general circulation over eastern Asia in summer, *Scientia Sinica.*, **17:** 397–420.